Faiza ABBA[1], M'hemed RACHEK[1]

Departement of Electrotechnics, Mouloud Mammeri University of Tizi Ouzou, Algeria (1)

doi:10.15199/48.2020.07.25

Non destructive evaluation based on time stepping finite element electromagnetic fields and mechanical structural deformation coupling models

Abstract. *The paper deal with high sensitive Non Destructive Testing of ferromagnetic materials based on the maximum mechanical structural deformation versus maximum eddy current electromagnetic force behaviors. Both physical quantities are computed from the transient electromagnetic fields and mechanical structural deformations models solved using the finite element method combined with the Newton–Raphson (N–R) algorithm. The proposed models are applied for an electromagnetic actuator (EMAs) evaluation through the comparison between the maximum deformation-maximum force profiles for healthy and geometrical defect cases under various lift-offs.*

Streszczenie. *W artykule przestawiono czułą metodę defektoskopii materiałów ferromagnetycznych bazującą na związku miedzy deformacją I prądami wirowymi. Do analizy defektów struktury wykorzystano metodę elementów skończonych oraz algorytm Newtona-Raphsona.* ***Metoda badań nieniszczących bazująca na analizie pola elektromagnetycznego, i związku między deformacją mechaniczną a prądami wirowymi.***

Keywords: Finite element method (FEM), Structural mechanical deformations, Non linear magnetic materials, Non destructive evaluation.
Słowa kluczowe: defektoskopia wiroprądowa, metoda elementów skończonych.

Introduction

Ferromagnetic materials in electromagnetic devices/actuators (EMDs/EMAs) are submitted to unwanted problems, such as vibration, acoustic noise and geometrical defects or properties degradations defects [1-4]. Although these phenomenon are mainly characterized by the coupled electromagnetic fields - mechanical equations [5, 6]. In this context, the multi-physics numerical analysis based on the Finite element method (FEM) is used to develop modern and cheaper innovative devices for use in investigations in the industry .Finite element method (FEM) is a widely used and well suited numerical method to solve electromagnetic field (EMF) include eddy current distribution and nonlinearity of materials and mechanical problems [7,9].

The paper investigate the relation between both the eddy current magnetic force density distribution and their impact on the structural deformation in order to characterize geometrical defects in conductive and ferromagnetic materials of electromagnetic actuators (Fig.1).The multilevel transient strong coupling tool is developed based on the finite element method (FEM), between transient magnetic and electric fields equations which are sequentially coupled to the mechanical structural dynamics through the magnetic force density. The eddy current equation expressed in terms of the magnetic vector potential (MVP) is coupled with the electric voltage-fed windings circuit equations obtained from Kirchhoff laws.

In addition, the (EMF) model integrates realistic geometries and the non-linear magnetic material properties through the magnetic flux density–magnetic permeability dependence handled by the iterative Newton–Raphson (N–R) method. In order to numerically predict the structural deformations, the mechanical behaviour of the ferromagnetic material is correlated with the volumic and surface magnetic forces densities distributions based on the Lorentz induced eddy current (LZEC) formulas, and computed from the time-stepping (N-R) electromagnetic coupled field model.

The presence of dimensional/properties defects in the electromagnetic devices modifies the magnetic flux density path and consequently exacerbate the no-homogeneous induced eddy currents petterns which initiate a major early failure of the pieces. The non destructive evaluation is studied through the maximum deformation according to the normal and tangential components of the magnetic force density, which allows the analysis of the mechanical deformation for small and large air gap for healthy and differents defects sizes. The developed multi-physics (EMF)–(MDef) time-stepping (FEM) model tools were implemented using the Matlab software.

Description of the Studied Actuators

As shown in Fig.1, the electromagnetic actuator is schematically consists of the two windings regions Ω_{coil} fed from voltage sources $V_{c1}(t)$ and $V_{c2}(t)$ with circulating current $I_{c1}(t)$ and $I_{c2}(t)$. The windings are mounted on ferromagnetic core Ω_{core}. The load region Ω_{load} is made of high-performance ferromagnetic material.

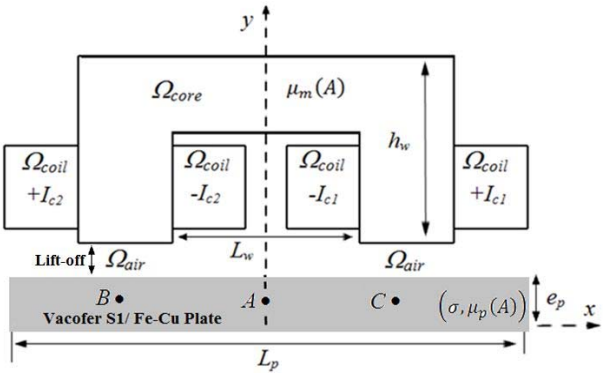

Fig.1. Typical components of the electromagnetic actuator.

Magnetic field and circuit equation (FEM) formulation

Extracted from Maxwell's equations, the transient magnetodynamic field model expressed in term of magnetic vector potential (MVP) which has only the z-direction component $\vec{A}(0,0,A_z)$ since the problem is two-dimensional (2D) in the *(x, y)* plane is given as follows:

$$\frac{\partial}{\partial x}\left(\frac{1}{\mu(A_z)}\frac{\partial A_z(x,y,t)}{\partial x}\right)+\frac{\partial}{\partial y}\left(\frac{1}{\mu(A_z)}\frac{\partial A_z(x,y,t)}{\partial y}\right) = \pm\frac{Nc}{S_c}I_c-\sigma\frac{\partial A_z}{\partial t} \quad (1)$$

where: I_c– the winding current, S_c –the total cross-sectional area of the winding turns, Nc – the number of turns,σ– the electric conductivity, $\mu(A_z)$ – the non-linear magnetic material permeability associated with the B–Hmagnetization curve.

The electric equation of the windings currents $I_{ck}(t)$ with the source voltages $V_{ck}(t)$ was obtained from the Kirchhoff law as follows:

$$V_{ck}(t)=R_c I_{ck}(t)+L_{end}\frac{dI_{ck}(t)}{dt}+$$

$$(2)\qquad \left[\sum_{m=1}^{N_c}\iint_{(S_c^m)^+}\frac{l}{(S_c^m)^+}\frac{dA_z}{dt}dS_c^+-\sum_{m=1}^{N_c}\iint_{(S_c^m)^-}\frac{l}{(S_c^m)^-}\frac{dA_z}{dt}dS_c^-\right]$$

where: $k=1,2$ – the windings number, $(R_c,\ L_{end})$ – the resistance and the self-inductance respectively.

After using the (FEM) discretization and the MVP approximation function in equations (1-2), the finite element formulation of the strong coupling between the electric circuit equation (2) with the (MVP)-based magnetic fields equation (1) leads to the differential first-order algebraic system of equations written as

$$(3)\qquad \begin{bmatrix} S(\upsilon) & -D_{s1} & -D_{s2}\\ 0 & R_c & 0\\ 0 & 0 & R_c\end{bmatrix}\begin{Bmatrix}[A_z]\\ I_{c1}\\ I_{c2}\end{Bmatrix}+\begin{bmatrix} T & 0 & 0\\ lN_s[D_{s1}]^{tr} & L_{end} & 0\\ lN_s[D_{s2}]^{tr} & 0 & L_{end}\end{bmatrix}\begin{Bmatrix}\frac{d[A_z]}{dt}\\ \frac{dI_{c1}}{dt}\\ \frac{dI_{c2}}{dt}\end{Bmatrix}=\begin{Bmatrix}[A_z]_{CL}^{\Omega}\\ V_{c1}(t)\\ V_{c2}(t)\end{Bmatrix}$$

where: $[A_z]$ –the nodal (MVP), $I_{c1}$and I_{c2} –the windings currents respectively.

The stifness matrix$[S]$,and the coupling matrices$[D_{S1}]$and$[D_{S2}]$are computed from the integral functions:

$$(4)\qquad S_{ij}^e(\mu(A_z))=\iint\frac{1}{\mu^e(A_z)}\left(\frac{\partial\alpha_i}{\partial x}\frac{\partial\alpha_j}{\partial x}+\frac{\partial\alpha_i}{\partial y}\frac{\partial\alpha_j}{\partial y}\right)d\Omega^e$$

$$(5)\qquad T_{ij}^{\ e}=\iint_{\Omega_{load}^e}\sigma\left(\alpha_i\alpha_j\right)d\Omega_{load}^e$$

$$(6)\qquad D_{ij}^e=\iint_{\Omega_{coil\,1,2}^e}\pm\frac{N_c}{S_c}(\alpha_i)d\Omega_{coil\,1,2}^e$$

In equation (3), the time derivatives of the vector potential and the winding currents are approximated by first-order difference ratios.

$$(7)\qquad \beta\frac{d}{dt}\begin{Bmatrix}[A_z]\\ I_{c1}\\ I_{c2}\end{Bmatrix}_{t+\Delta t}+(1-\beta)\frac{d}{dt}\begin{Bmatrix}[A_z]\\ I_{c1}\\ I_{c2}\end{Bmatrix}_{t}=\frac{\left(\begin{Bmatrix}[A_z]\\ I_{c1}\\ I_{c2}\end{Bmatrix}_{t+\Delta t}-\begin{Bmatrix}[A_z]\\ I_{c1}\\ I_{c2}\end{Bmatrix}_{t}\right)}{\Delta t}$$

where: Δt –the length of the time steps, β –constant defining the time integration schema. They have $(\beta=3/2)$a value of Galerkine methodfor the used in this work.

The first ordrer time-derivative approximation of the vector potential and winding currents in adition to the non-linear magnetization $B(H)$curve need the use of the time stepping schems associated to the Newton-Raphson (N-R) algorithm[7,8].Then algebraic equation system (3) becomes :

$$\left(\beta\begin{bmatrix} P\left(\mu\left(A_z^{k+1}\right)\right)+\frac{[T]}{\Delta t} & -D_{s1} & -D_{s2}\\ \frac{lN_s[D_{s1}]^{tr}}{\Delta t} & R_c+\frac{L_{end}}{\Delta t} & 0\\ \frac{lN_s[D_{s2}]^{tr}}{\Delta t} & 0 & R_c+\frac{L_{end}}{\Delta t}\end{bmatrix}\right)\begin{Bmatrix}\Delta A_z\\ \Delta I_{c1}\\ \Delta I_{c2}\end{Bmatrix}_{t+\Delta t}^{k+1}=$$

$$-\left((\beta)\begin{bmatrix} S\left[\mu\left(A_z^k\right)\right]+\frac{[T]}{\Delta t} & -D_{s1} & D_{s2}\\ \frac{lN_s[D_{s1}]^{tr}}{\Delta t} & R_c+\frac{L_{end}}{\Delta t} & 0\\ \frac{lN_s[D_{s2}]^{tr}}{\Delta t} & 0 & R_c+\frac{L_{end}}{\Delta}\end{bmatrix}\right)\begin{Bmatrix}\Delta A_z\\ \Delta I_{c1}\\ \Delta I_{c2}\end{Bmatrix}_{t+\Delta t}^{k}$$

$$+\left((1-\beta)\begin{bmatrix} S\left(\mu\left(A_z^k\right)\right) & -D_{s1} & -D_{s2}\\ -\frac{lN_s[D_{s1}]^{tr}}{\Delta t} & R_c+\frac{L_{end}}{\Delta t} & 0\\ -\frac{lN_s[D_{s2}]^{tr}}{\Delta t} & 0 & R_c+\frac{L_{end}}{\Delta t}\end{bmatrix}\right)\begin{Bmatrix}\Delta A_z\\ \Delta I_{c1}\\ \Delta I_{c2}\end{Bmatrix}_{t}$$

$$(8)\qquad +\begin{Bmatrix}[A_z]_{CL}^{\Omega}\\ \beta V_{c1}(t+\Delta t)+(1-\beta)V_{c1}(t)\\ \beta V_{c2}(t+\Delta t)+(1-\beta)V_{c2}(t)\end{Bmatrix}$$

The Jacobian matrix system $[P]$in equation (8) is given by the following matrix elements (9):

$$(9)\qquad P_{ij}^e=\iint_{\Omega^e}\left[\frac{\partial}{\partial A_{zj}}\left(\frac{1}{\mu\left(A_{zj}\right)}\right)\right]\cdot\left(\vec{\nabla}\alpha_i\bullet\vec{\nabla}\alpha_j\right)\cdot d\Omega^e$$

To update the iterativevalues of the nodal magnetic vector potential, the relaxation $0.5\le\theta\le1$factor may be used.

Calculation of magnetic eddy current forces

There are several physical or mathematical representations methods to formulate the volume f_V and surface f_S electromagnetic forces densities exerted on a ferromagnetic medium [10-12] .The Korteweg Helmholtz force density f^{em} for a magnetic plate in (x,y) plane is expressed as:

$$(10)\qquad f^{em}=f_V^{em}+f_S^{em}=\mu\left(A_z\right)\left(\vec{J}_{eddy}\times\vec{H}\right)+\left[-\frac{1}{2}\left(H_x^2+H_y^2\right)\nabla\mu\right]$$

where: H_x and H_y –are the tangential and normal magnetic field located on the plate surrounding the surface. J_{eddy} – The induced eddy current.

The components of the volume magnetic force density components(f_{Vx},f_{Vy})expressed from the Lorentz eddy current force (LZEC) formulas in non-linear magnetic material (NL) can be written as follows for the 2D(x,y)plane at each step time:

$$\left[f_V^{em}\right]=\begin{bmatrix}f_{Vx}\\ f_{Vy}\end{bmatrix}_{t+\Delta t}=\mu(A_z)\left(\vec{J}_{eddy}\times\vec{H}\right)_{t+\Delta t}$$

$$(11)\qquad =\left[\frac{\beta-1}{\beta}\left(J_{eddy}\right)_t-\sigma\frac{\left(A_z^e\right)_{t+\Delta t}-\left(A_z^e\right)_t}{\beta\Delta t}\right]\begin{bmatrix}\left(\frac{\partial A_z^e}{\partial x}\right)\vec{i}\\ \left(\frac{\partial A_z^e}{\partial y}\right)\vec{j}\end{bmatrix}_{t+\Delta t}$$

The tangential and normal component of the surface magnetic force density(f_{Sx},f_{Sy}) expressed from the Maxwell stress tensor formulas for ferromagnetic material with high magnetic permeability is written as:should be as:

(12) $$f_S^{em}=\begin{bmatrix}f_{Sx}\\ f_{Sy}\end{bmatrix}=\begin{bmatrix}0\cdot\vec{i}\\ -\frac{1}{2}\left(\frac{1}{\mu_p(A_z)}-\frac{1}{\mu_o}\right)B_y^2\cdot\vec{j}\end{bmatrix}=\begin{bmatrix}0\cdot\vec{i}\\ \frac{1}{2}\left(\frac{1}{\mu_o}-\frac{1}{\mu_p(A_z)}\right)\left(\frac{\partial A_z}{\partial x}\right)^2\cdot\vec{j}\end{bmatrix}$$

Mechanical deformation FEM formulation model

Coupled electromagnetic fields in ferromagnetic media induce volume and surface electromagnetic force density sources occurring in the mechanical equilibrium equations [12-14]. According to (2D) *(x,y)* cartesian coordinate system, the structural mechanical equilibrium differential equation expresses the relationship between the mechanical stress components and the magnetic force density when assuming small deformations and non-dynamic behavior due to the inertia can be written as:

(13) $$\begin{cases}\frac{\partial\sigma_{xx}}{\partial x}+\frac{\partial\sigma_{xy}}{\partial y}+f_{Vx}^{em}=0\\ \frac{\partial\sigma_{xy}}{\partial x}+\frac{\partial\sigma_{yy}}{\partial y}+f_{Vy}^{em}=0\\ \sigma(U)\bullet n=f_S^{em}\end{cases}$$

where: $\sigma_{xx},\sigma_{yy},\sigma_{xy}$– the stresses along the x, y and xy-directions, respectively, $\sigma(U)$ – the mechanical stress tensor, U – the displacement vector.

From the concepts of stress and strain, the generalized Hook's law states that the components of stress are linearly related to the components of strain .The generalized stress $\{\sigma\}$-strain $\{\varepsilon\}$relation given by the Hook's law in the case of linearity elastic isotopic (2D) solid is written as:should be as:

(14) $$\{\sigma\}^T=\begin{Bmatrix}\sigma_{xx}\\ \sigma_{yy}\\ \sigma_{xy}\end{Bmatrix}=\begin{pmatrix}\frac{E}{1-\nu^2} & \frac{E\nu}{1-\nu^2} & 0\\ \frac{E\nu}{1-\nu^2} & \frac{E}{1-\nu^2} & 0\\ 0 & 0 & \frac{E(1-\nu)}{2(1-\nu^2)}\end{pmatrix}\begin{Bmatrix}\varepsilon_{xx}\\ \varepsilon_{yy}\\ \varepsilon_{xy}\end{Bmatrix}=[G]_{3\times3}\{\varepsilon\}$$

where: E – Young's modulus, ν – Poisson's ratio.

According to the consideration of small deformations, the linear strain deformation–displacement relationships expressed in general matrix form as follows:

(15) $$\{\varepsilon\}^T=\begin{Bmatrix}\varepsilon_{xx}\\ \varepsilon_{yy}\\ \varepsilon_{xy}\end{Bmatrix}=\begin{Bmatrix}\frac{\partial u(x,y)}{\partial x}\\ \frac{\partial v(x,y)}{\partial y}\\ \frac{\partial u(x,y)}{\partial y}+\frac{\partial v(x,y)}{\partial x}\end{Bmatrix}$$

Discretization by (FEM)of the mechanical part of the equations (13) applying the weighted residual method and applying the substitution of the constitutive equation (stress–strain) gives us: should be as:

(16) $$\int_{\Omega_{load}}\begin{Bmatrix}\Psi_1\left(\frac{\partial\sigma_{xx}}{\partial x}+\frac{\partial\sigma_{xy}}{\partial y}\right)\\ \Psi_2\left(\frac{\partial\sigma_{yx}}{\partial x}+\frac{\partial\sigma_{yy}}{\partial y}\right)\end{Bmatrix}d\Omega_{load}-\int_{\Omega}\begin{Bmatrix}\Psi_1 f_{Vx}\\ \Psi_2 f_{Vy}\end{Bmatrix}d\Omega_{load}-\int_{\Gamma_{load}}\begin{Bmatrix}\Psi_1 f_{Sx}\\ \Psi_2 f_{Sy}\end{Bmatrix}d\Gamma_{load}=0$$

where: Ω_{load} –the mechanical domain of the plate, Γ_{load} – the boundary ofΩ_{load}, $\Psi_1 and\ \Psi_2$– are the weighting functions.

After substitution of the stress–tensor equation (14) and the strain–displacement equation (15) into equation (16), and interpolating the body displacements using the (FE) shape functions, this gives:

$$\frac{E}{1-\nu^2}\begin{bmatrix}\frac{\partial\Psi_1}{\partial x} & \nu\frac{\partial\Psi_1}{\partial x} & \left(\frac{1-\nu}{2}\right)\frac{\partial\Psi_1}{\partial y}\\ \nu\frac{\partial\Psi_2}{\partial y} & \frac{\partial\Psi_2}{\partial y} & \left(\frac{1-\nu}{2}\right)\frac{\partial\Psi_2}{\partial x}\end{bmatrix}$$

(17) $$\int_{\Omega_{load}^e}\times\begin{bmatrix}\frac{\partial\alpha_1}{\partial x} & 0 & \frac{\partial\alpha_2}{\partial x} & 0 & \frac{\partial\alpha_3}{\partial x} & 0\\ 0 & \frac{\partial\alpha_1}{\partial y} & 0 & \frac{\partial\alpha_2}{\partial y} & 0 & \frac{\partial\alpha_3}{\partial y}\\ \frac{\partial\alpha_1}{\partial y} & \frac{\partial\alpha_1}{\partial x} & \frac{\partial\alpha_2}{\partial y} & \frac{\partial\alpha_2}{\partial x} & \frac{\partial\alpha_3}{\partial y} & \frac{\partial\alpha_3}{\partial x}\end{bmatrix}\begin{Bmatrix}u_1\\ v_1\\ u_2\\ v_2\\ u_3\\ v_3\end{Bmatrix}d\Omega_{load}^e=\int_{\Omega_{load}^e}\begin{Bmatrix}\Psi_1 f_{Vx}\\ \Psi_2 f_{Vy}\end{Bmatrix}d\Omega_{load}^e+\int_{\Gamma_{load}^e}\begin{Bmatrix}\Psi_1 f_{Sx}\\ \Psi_2 f_{Sy}\end{Bmatrix}d\Gamma_{load}^e$$

where: $\alpha(x,\ y)$ – the shape function associated with the displacements of the nodes *(j=1,2,3)* of each triangular element *j*.

As a result, the stiffness matrix *[K]* and magnetic force density vector *[F]* build the global algebraic equations system written as:

(18) $$[K]\{U\}=[F_V]+[F_S]=[F]$$

According to equation (17), the elementary stiffness matrix of the algebraic system in equation (18) is expressed as follows:should be as:

(19) $$[K_{ij}]=\int_{\Omega_{load}^e}[B]^T[G][B]d\Omega_{load}^e$$

Numerical Implementation

In this part, we present the results of the simulations obtained from the computation code analysis package of the coupled magnetic, electrical and mechanical equations models,developed and solved by the nodal based (FEM) tools implemented under Matlab software.Physical boundary conditions are imposed according to electromagnetic field and mechanical deformation models as depicted in Fig. 2.

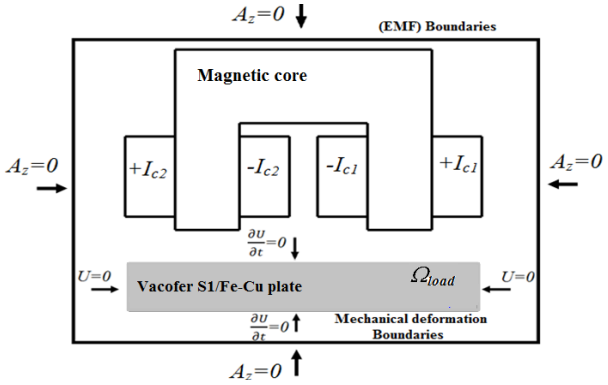

Fig.2. Electromagnetic and mechanical deformation boundary condition.

The relevant geometrical and physical propertiesof the actuators is presented in Table1. The dimensions of the simulated samples under geometrical defectsare explainedand given in Fig. 3 and Table 2 respectively.

Table 1. Physical and geometrical parametrers of the actuators

Electrical and Mechanical Parameters	Values	Geometrical Parameters	Values [mm]
Young Modulus (E)	200 KN/mm2	Plate Length(Lp)	170
Poisson Ration(υ)	0.33(Vacofer S1) 0.24(Fe-Cu alloy)	Plate Thickness(e_p)	15
Winding Resistance (Rc)	1Ω	Lift-off	1-5
Winding Inductance (L_{end})	5mH	Winding Width(hw)	37
Plate Electrical conductivity (unit MS/m)	10.21(Vacofer S1) 9.1 (Fe-Cu alloy)	Winding Length(Lw)	15
Supply voltage (V)	40V	–	–

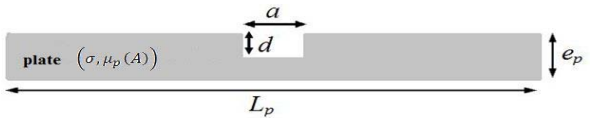

Fig.3. Studied of plate configuration defect.

Table 2. Different dimensions of the simulated defects

Defects dimensions	Length (a) [mm]	Depth (d) [mm]
Defect 1	6	0.75
Defect 2	6	1
Defect 3	10	1
Defect 4	6	1.25

The results of coupled magneto-electrical simulations (FEM)

At each step timeof Δt=1ms, the algebraic system in equation (8) corresponding to the electromagnetic model based (2D)-(FEM) transient andNewton–Raphson algorithm was iteratively solved to obtain the node values of the magnetic vector potential and the winding current at each time step, according to the actual magnetic permeability values.

Fig.4.shows the equipotential lines of the steady state magnetic vector potential nodal values, which are particularly concentrated on the cross section of the plate faced to the magnetic core and excited coils.

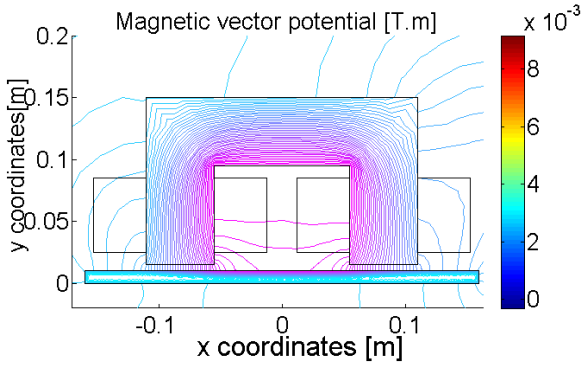

Fig.4. Steady state distribution of the magnetic vector potential at t=0.05s.

The field line distribution and the magnetic flux density map-vectors are plotted in Fig.5 . The maximum value of magnetic flux density in the plate domain is about 1.6 T which corresponds to the nonlinear region of the B-H curve associated to the Vacofer S1 material.The associated coil currents are given in Fig.6 .

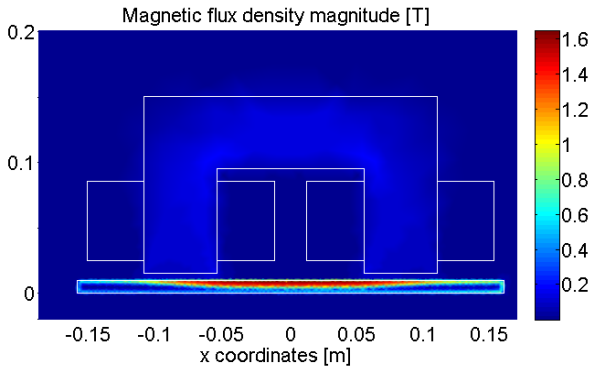

Fig.5. Steady state of the magnetic flux density spatial distribution.

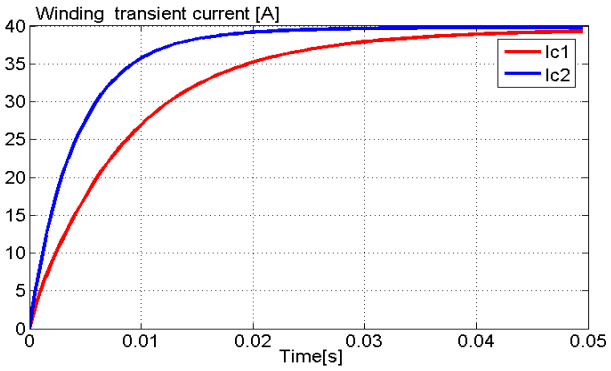

Fig.6. Winding transient current.

The magnetic force density map vectors are plotted in Fig. 7, in where we note a significant force density in the middle of the plate.

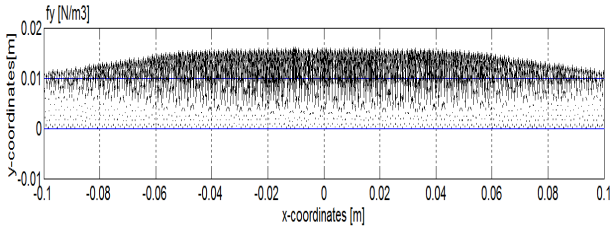

Fig.7. Steady state of the magnetic force density: vector field orientation.

Fig. 8 and Fig. 9 shows respectively the maximums induced eddy current density and magnetic force density behavior of non linear magnetic materials according with x-coordinates for different electrical conductivity (Vacofer S1 and Fe-Cu alloy material).The highest electrical conductivity lead to highest eddy current and magnetic force density values.

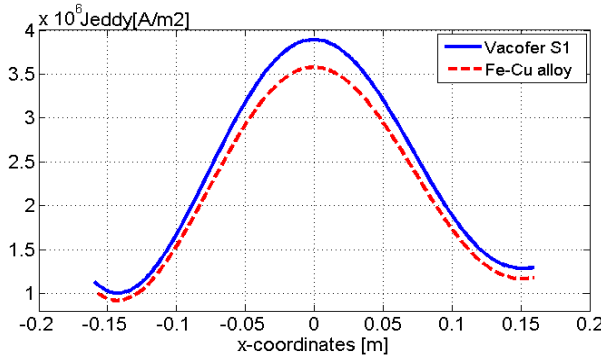

Fig.8 Maximum eddy current density as function x-coordinates for two ferromanetic material.

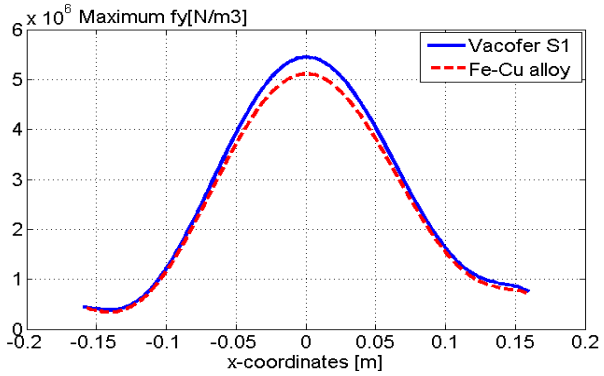

Fig.9. Maximum magnetic force density as function x-coordinates for two ferromagnetic materials.

Fig.10 show the time variation of the maximum values of the nonlinear magnetic force density in the positions A(0mm, 9.5mm), B(25mm, 9.5mm), and C(−25mm,9.5mm) of the Vacofer plate. The peak values of the volume magnetic force density fy-components were positive and about 5.5 MN/m^3 and 2 MN/m^3 ,respectively for the A, B and C points of the plate at the lift-off=5mm. A maximum magnetic force density occurs around the 7ms time. These non-linear force–eddy current–magnetic flux density and force–magnetic permeability relation ships and the high force variation were the major reasons for the production of large forces, which allowed a design with a large deformation.

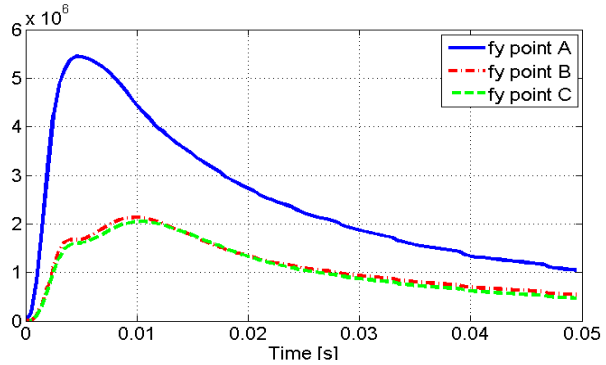

Fig.10. Transient magnetic force density in the nonlinear magnetic materials obtained with three points in the Vacofer S1 plate.

Fig.11 and Fig.12 present respectively the transient maximum nonlinear magnetic force density at healthy and different geometrical defects according to the lift-off.The nonlinear magnetic force density is greatly affected by the reduced of the lift-off and defects presence. Increased of the defects shape lead to the increased of the magnetic force density of the region surrounding the defect.

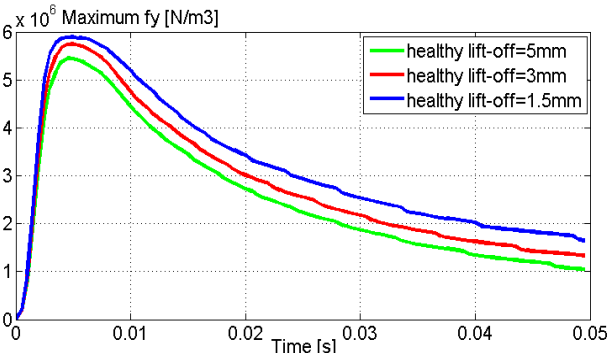

Fig.11. Transient magnetic force density in healthy Vacofer S1 Plate with differents lift-offs.

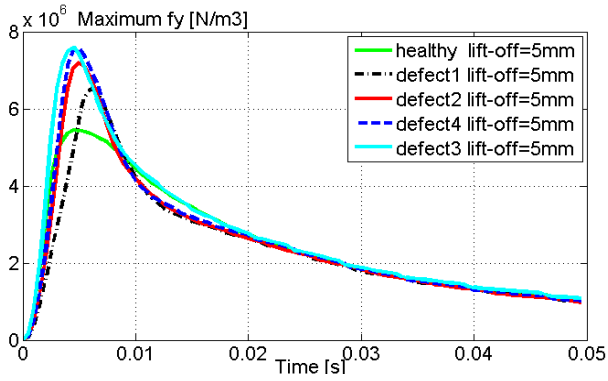

Fig.12. Transient magnetic force density inhealthy and faulty Vacofer S1 plate at lift-off=5mm.

The results of mecanical problem simulations (FEM)

In this section, we performed a transient (FEM) mechanical–structural deformation analysis of the conducting magnetic plate under the nonlinear magnetic force density excitation. Special attention was paid to the moments that the magnetic force densities reached a maximum, which caused significant deformations on the plate. The structural mechanical deformation equation was sequentially coupled to the electromagnetic equations through the nonlinear magnetic force density under the independent (EMF) and mechanical meshes.

The (FEM) analysis of the mechanical structural deformation model allowed us to identify the most stressed areas of the previous elements whose shape was appropriately designed so as to reduce the maximum stresses and deformations. The obtained time results of the maximum deformation-maximum magnetic force density profiles of the nonlinear magnetic material Vacofer S1 for healthy and geometrical defect cases under various lift-offs were presented in Fig. 13 and Fig. 14.

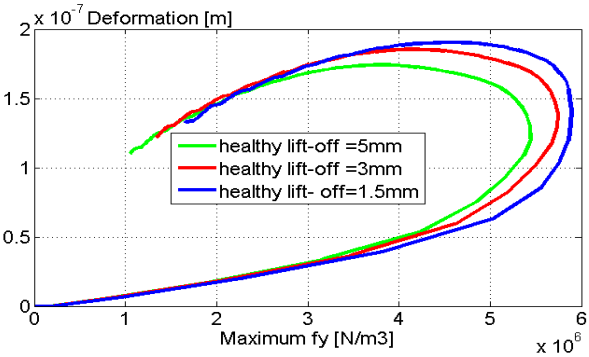

Fig.13. Maximum deformation ε_{xy} in healthy Vacofer S1 plate with different lift-offs.

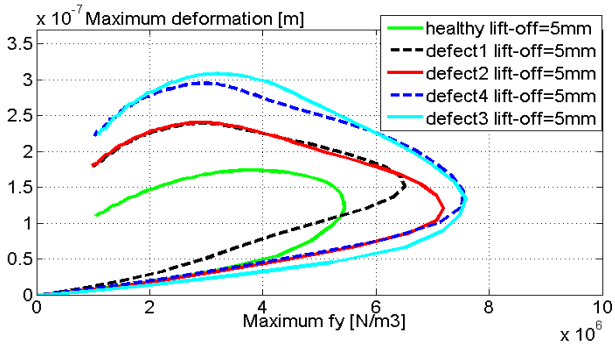

Fig.14. Maximum deformation ε_{xy} in healthy and faulty Vacofer S1 plate at lift-off=5mm.

Fig.13 shows that reduced lift-off leads to increased values of stress and repetitive deformations, which could exceed the fatigue limit of the plate. In Fig.14 the maximum value of the deformation increased with the increased defects shape. As the materials electrical conductivity and nonlinear magnetic properties are highest, the mechanical deformation is greatly affected by the defects through increased and exceeds random distribution of the magnetic force density.

Table 3 summarizes the peak values of the maximum nonlinear magnetic force density f_y component and the ε_{xy} deformation for the different lift-offs at healthy and defect cases for the Vacofer S1 nonlinear magnetic material.

Table 3. Peak values of the magnetic force density and deformation according to the lift-off at healthy and defect cases.

Lift_offs [mm]		f_y magnetic eddy current force density [MN/m^3]	ε_{xy} deformation (peak values) [μm]
1.5 (healthy)		5.8927	0.1907
3(healthy)		5.7462	0.1857
5	healthy	5.4465	0.1744
	defect1	6.5154	0.2398
	defect2	7.1957	0.2408
	defect3	7.5970	0.3088
	defect4	7.5488	0.2956

Conclusion

The paper has proposed detailed pulsed transient-voltage electromagnetic fields and structural mechanical deformation coupled models based finite element method in order to establish the kind between the maximum mechanical deformation-maximum force profiles named the mechanical deformation impedance which allows to a non destructive testing of ferromagnetic materials used in electromagnetic actuators (EMAs), under the healthy and geometrical local defects with different lift-off. The computed magnetic force density and structural deformation results obtained from the coupled (FEM) magnetic field–electric circuit and mechanical structural deformation models were qualitatively in good agreement with the models found in the scientific literature.

The developed models are a promising contribution in the area of the non-destructive testing, safety, and threatened by wake-induced fatigue due to repetitive deformation strain activated by a pulsed voltage source.

***Authors**: PhD student, Faiza Abba, Department Electrotechnics, Mouloud Mammery University of Tizi-Ouzou ,BP 15000,Algeria,Email: aba-faiza@hotmail.com; Dr. M'hemed Rachek, Department Electrotechnics, Mouloud Mammery University of Tizi-Ouzou, BP 15000, Algeria, and Email:rachek_mhemed@yahoo.fr.*

REFERENCES

[1] Belahcen A., Vibration of Rotating Electrical Machines due to Magnetomechanical coupling and Magnetostriction, *IEEE Transactions on Magnetics*., 42 (2006), No.4, 974-974.

[2] Podhajecki J.,Mlot A., Korkosz M., Resina E., Arrkio A.;Comparison Vibration due to Maxwell Forces and Magnetostriction in BLDC Motors, *Przegląd Elektrotechniczny(Elecrical review)*., 62 (2008), No. 28, 325-330.

[3] Pengpeng S., Xiaojing Z., Magnetic Charge Model for 3D MMM Signals, *Non desructive Testing and Evaluation* ., 31 (2016), No. 1, 45-60

[4] Hilgert T., Vandevelde L., Melkebeek J., Magnetostriction Measurements on Electrical Steels by Means of Strain Gauges and Numerical Applications, *Przegląd Elektrotechniczny(Elecrical review)*., 81 (2005), No. 5, 87-91.

[5] Aydin U., Rasilo P., Martin F., Singh D., Daniel L., Belahcen A., Arrkio A; Magneto-Mechanical Modeling of Electrical Steel Sheets, *Journal of Magnetism and Magnetic Materials*, *Journal of Magnetism and Magnetic Materials*., 439 (2017),82-90.

[6] Fonteyn K., Belahcen A., Kouhia R., Rasilo P.,Arkkio A., FEM for Directly Coupled Magneto-Mechanical Phenomena in Electrical Machines, *IEEE Trans. Magn*., 46 (2010), No. 8, 2923-2926.

[7] Marzouki T., Rachek M., Finite Element Method Applied to the Modellig and Analysis of Induction Motors, In: *Numerical Modelling*. Intech Open, 2012.

[8] Isfahani A. H., Vaez-Zadeh S.,Khodabakhsh A. N., Calculation of Maximum short Circuit Electromagnetic Forces in the IPB using time Stepping Finite Element Method,*Przegląd Elektrotechniczny(Elecrical review)*., 85 (2009), No. 7, 31-35

[9] Arrkio A., Pike G.E., Analysis of Induction Motors Based on the Numerical Solution of the Magnetic Field and Circuit Equations, Ph.D.dissertation, Helsinki University of Technology,.1987.

[10] Lee S.H.; He, X.; Kim, D.K.; Elborai, S.; Choi, H.S. Park, I.H.; Zahn, M., Evaluation of the Mechanical Deformation in Incompressible Linear and Nonlinear Magnetic Material Using Various Electromagnetic Force Density Methods, *J.Appl. Phys*., 97 (2005), No. 10, 10E108.

[11] Clausse B., Modélisation des Traducteurs Electromagnetiques Acoustiques (EMAT) pour le Controle Non-Destructif (CND) de Milieux Ferromagnétiques, Ph.D.Thesis, University Paris-SACLAY, 2018.

[12] Belahcen A., Magneoelasticity, Magnetic Forces and Magnetostriction in Electrical machines, Ph.D.Thesis,Helsinki University of Technologie, 2004.

[13] Ren Z.; Ionescu B.; Besbes M.; Razek A., Calculation of Mechanical Deformation of Magnetic Materials in Electromagnetic Devices, *IEEE Trans. Magn*., 31 (1995), 1873-1876.

[14] Galopin N., Azoum K., Besbes M., Bouillault F., Daniel L., HubertO., Alves F., Pike G.E., Caractérisation et Modélisation des Déformations Induites par les Forces Magnétiques et par la Magnétostriction, *Revue internationale de génie électrique*. 9 (2006), No. 4, 499-514.